Title	Influence of Input Energy Density on Morphology of Unique Layered Microstructure of γ-TiAl Alloys Fabricated by Electron Beam Powder Bed Fusion
Author(s)	Cho, Ken; Morita, Naohide; Matsuoka, Hiromasa et al.
Citation	Materials Transactions. 2023, 64(1), p. 44-49
Version Type	VoR
URL	https://hdl.handle.net/11094/89909
rights	
Note	

Materials Transactions, Vol. 64, No. 1 (2023) pp. 44 to 49
Special Issue on Recent Research and Development in the Processing, Microstructure, and Properties of Titanium and Its Alloys

Influence of Input Energy Density on Morphology of Unique Layered Microstructure of γ-TiAl Alloys Fabricated by Electron Beam Powder Bed Fusion[*1]

Ken Cho[1,2], Naohide Morita[1], Hiromasa Matsuoka[1], Hiroyuki Y. Yasuda[1,2,*2], Mitsuharu Todai[3], Minoru Ueda[4], Masao Takeyama[5] and Takayoshi Nakano[1,2]

[1] *Graduate School of Engineering, Osaka University, Suita 565-0871, Japan*
[2] *Anisotropic Design & Additive Manufacturing Research Center, Graduate School of Engineering, Osaka University, Suita 565-0871, Japan*
[3] *Department of Environmental Materials Engineering, Institute of Niihama National College of Technology, Niihama 792-8580, Japan*
[4] *Metal Technology Co. Ltd., Tokyo 164-8721, Japan*
[5] *Department of Metallurgy and Ceramics Science, Tokyo Institute of Technology, Tokyo 152-8550, Japan*

Microstructure and tensile properties of Ti–48Al–2Cr–2Nb (at%) rods fabricated by electron beam powder bed fusion (EB-PBF) process were investigated by changing input energy density (*ED*) which is one of the important factors affecting formation of the melt pool. We found that unique layered microstructure consisting of an equiaxed γ grain layer (γ band) and a duplex region can be formed by EB-PBF with *ED* in the range of 13 to 31 J/mm^3. It is interesting to note that the width of the γ band and the volume fraction of the γ phase in the duplex region decrease with increasing *ED*. On the other hand, the α_2/γ lamellar grain in the duplex region increases with increasing *ED*. These morphological changes in the layered microstructure are attributed to variation of temperature distribution from melt pool caused by increasing *ED*. Moreover, we also found for the first time the strength of the alloys can be improved by decreasing width of the γ band and increasing of the α_2/γ lamellar grain in the duplex region. Whereas, the width of the γ band and the fraction of the equiaxed γ grain in the duplex region should be increased to enhance ductility of the alloys. [doi:10.2320/matertrans.MT-MLA2022015]

(Received June 28, 2022; Accepted August 18, 2022; Published December 25, 2022)

Keywords: *additive manufacturing, titanium aluminide, energy density, microstructure control, tensile property*

1. Introduction

Metal 3D printing which is referred to as metal additive manufacturing (AM) has attracted attention in recent years.[1–3] Metal components have mainly been fabricated by machining, die forging or casting to this day. These conventional fabrication methods are called as subtractive manufacturing because the excess portions of materials are removed to obtain the desired shape of the final parts. On the other hand, in metal AM, the desired component is fabricated by melting and layering metal powders based on 3D-CAD data. Powder bed fusion (PBF) is a metal AM technique in which metal powder beds are selectively melted and solidified using focused electron or laser beams as heat sources. The PBF is a prospective next-generation manufacturing method for fabricating complex and custom-shaped metal components for aerospace and medical device.[4–6] Thus, fabrication technologies using the PBF have been developed for several varieties of structural materials, such as Ti alloys,[7–9] Ni-based superalloys,[10–12] stainless steels[13,14] and γ-TiAl alloys.[15–17]

Another important feature of PBF is unique microstructures induced by unusual solidification conditions, thermal history and scan strategies including directional or orthogonal scans during the process.[18–27] For example, it has been reported that the shape of the melt pool and the solidification speed during the PBF processes of Ti alloys[28–33] and Ni-based superalloys[34–36] can be controlled using appropriate process conditions and scanning strategies. Consequently, a single-crystal-like microstructure or a unique crystallographic lamellar microstructure can be obtained. The alloys with these unique microstructures exhibit excellent mechanical properties than conventional alloys. These reports suggest that the PBF is a useful process for controlling the shape and mechanical properties of the metal components.

γ-TiAl alloys are light-weight heat-resistant alloys that are composed of Ti_3Al (α_2), TiAl (γ) and TiAl (β) phases with the $D0_{19}$, $L1_0$ and B2 structures, respectively. These alloys are expected to replace Ni-based superalloys because of their excellent specific strength. In general, the microstructures of Ti-rich TiAl alloys depend strongly on the heat treatment temperature as follows: (i) a fully α_2/γ lamellar structure, (ii) a duplex structure and (iii) a near γ structure. The α_2/γ lamellar structure that satisfies the Blackburn orientation relationship is known as a strengthening structure of γ-TiAl alloys. The duplex structure is composed of fine equiaxed γ and α_2/γ lamellar grains. It is important to note that the mechanical properties of the alloys can be improved by controlling the morphologies of these microstructures. Our research group has developed fabrication processes for γ-TiAl alloy components using the electron beam powder bed fusion (EB-PBF),[37–43] focusing on the shape and microstructure. In EB-PBF, high-melting-point metallic materials can be fabricated in vacuum using an electron beam as the heat source. The input energy density (*ED*) of EB-PBF can be controlled by varying the process conditions such as beam current and scanning speed according to the following equation,

$$ED = \frac{I \times U}{v \times h \times d} \tag{1}$$

where I is the beam current, U is the beam voltage, v is the scanning speed, h is the scanning pitch and d is the layer thickness. By varying *ED*, the maximum temperature and the

---

[*1] This Paper was Originally Published in Japanese in J. JILM **72** (2022) 298–303.

[*2] Corresponding author, E-mail: hyyasuda@mat.eng.osaka-u.ac.jp

temperature gradient at the melt pool and temperature distribution of its vicinity can be altered significantly, which in turn affects the structural integrity and microstructure of the specimens.[44,45] In a previous study using the β phase-containing γ-TiAl alloy, it was found that a massive α transformation can be induced by an increase in cooling rate near the melt pool at lower *ED*.[41] Through this massive α transformation, an ultrafine α_2/γ lamellar structure with a lamellar spacing of only approximately 30 nm can be obtained. The alloys with ultrafine lamellar grains show greater high-temperature strength than cast alloys.[41,42] Furthermore, we also found out that it is possible to fabricate Ti–48Al–2Cr–2Nb (at%, hereafter 4822) alloys with a unique layered microstructure composed of the duplex structure and near γ structure regions.[37,43] The near γ structure region is referred to as the γ band. The formation of the layered microstructure is closely related to the repetition of melting of raw powders and a temperature distribution from melt pool formed at each melting. Therefore, the layered microstructure can be oriented in any direction by changing the building direction. In particular, the alloy with the layered microstructure oriented 45° to the loading direction shows excellent high-temperature strength and fatigue strength.[38,39] Even more importantly, it overcomes the low ductility issue, which has been challenging for conventional alloys.[37,40] These previous studies imply that the mechanical properties of the alloys with the layered microstructure depend strongly on the morphologies of the γ band and duplex region. However, the relationship between process conditions and the morphology of the layered microstructure has not been clarified in detail. Thus, the purpose of this study is to quantitatively investigate the effects of *ED* on the morphology of the layered microstructure of 4822 alloys, focusing on the width of the γ band and the volume fractions of the γ and α_2/γ lamellar grains in the duplex region. In addition, their effects on the strength and ductility of the alloy at room temperature were examined.

2. Experimental Procedure

Cylindrical rods, 90 mm in length and 10 mm in diameter, were prepared by EB-PBF using gas-atomized 4822 alloy powder. The average particle diameter of the raw powder is around 100 µm. The layer thickness was 90 µm, and the longitudinal direction of the rods was set parallel to the building direction (Fig. 1(a)). Furthermore, *ED* that can be determined using eq. (1) was set to 13, 20 and 31 J/mm^3. Hereafter, samples fabricated at different *ED* are referred to as low *ED* rod (13 J/mm^3), medium *ED* rod (20 J/mm^3) and high *ED* rod (31 J/mm^3). The defect ratio originating from a lack of fusion is less than 1.5% (low *ED* rods: 1.5%, medium *ED* rods: 1.3% and high *ED* rods: 1.2%). The porosity derived from the atomization gas trapped in the raw powder (Ar gas pore) is less than 0.6% (low *ED* rod: 0.5%, medium *ED* rod: 0.6%, and high *ED* rod: 0.2%). Here, it should be noted that all rods used in this study were not subjected to aging or hot isostatic pressing (HIP) treatments.

The longitudinal section of each rod was observed by a scanning electron microscopy (SEM) for microstructure analysis. The specimens for the SEM observation were mechanically polished with waterproof emery papers of up to #2000 grit and subsequently electrically polished in a $HClO_4$: butanol: methanol (6:35:59 vol%) solution. The microstructure was quantitatively investigated using the image analysis software ImageJ. Four SEM images at ×600 magnification were used for this analysis, and the mean value and standard deviation of each evaluation parameter that characterizing the morphology of the layered microstructure were obtained.

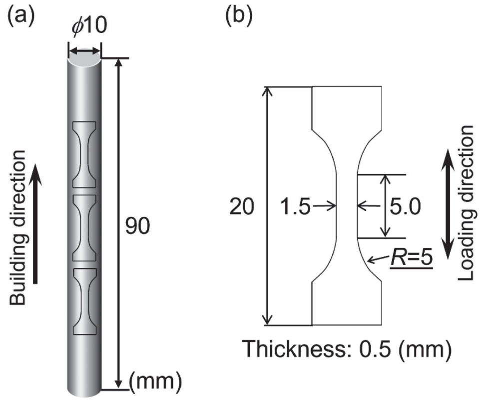

Fig. 1 Schematic drawings of the 4822 alloy rods fabricated by the EB-PBF (a) and the specimens for tensile tests (b).

To evaluate the tensile properties of the rods, tensile test specimens were cut from each rod with the longitudinal direction as the load axis direction, as shown in Fig. 1(a). The dimensions of the tensile specimen are presented in Fig. 1(b). Tensile tests were conducted under vacuum at room temperature at a strain rate of $1.7 \times 10^{-4}\,s^{-1}$. Tensile tests were conducted at least three times for each rod, and yield stress (σ_y) and elongation (*EL*) were obtained from the average of these tests. In addition, the nanoindentation hardness of the γ-band and the duplex region was investigated by nanoindentation tests. The maximum load was set to 58.8 mN, and the hardness of each region was calculated from the average of measurements taken at more than 10 locations. The specimens for the mechanical tests were polished mechanically using both waterproof emery papers and a colloidal SiO_2 suspension.

3. Results and Discussions

3.1 Influence of input energy density on microstructure

Figure 2 shows the microstructures at approximately 70 mm from the bottom of the rods fabricated at different *ED*. In these SEM images, the γ and α_2 phases show gray and white contrasts, respectively. It should be noted that no height dependence was observed in the microstructure of all rods. As shown in Fig. 2, the layered microstructure composed of the duplex region and the γ band is formed perpendicular to the building direction, regardless of *ED*. The mean diameter of the equiaxed γ grains in the γ band is approximately 10 µm (Fig. 2(a), (b), (d)). The grain size of the duplex region is much smaller than that of the γ band. The equiaxed γ and α_2/γ lamellar grains have mean diameters of approximately 10 µm or less. Moreover, the granular α_2 phase is just 1 µm or less (Fig. 2(d), (e), (f)). The

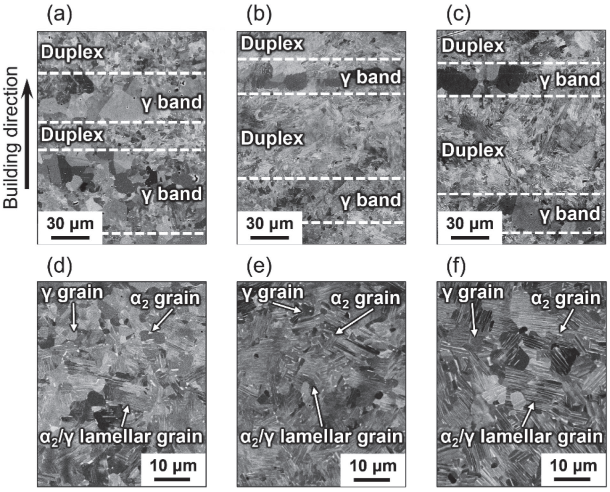

Fig. 2 Typical SEM images of low *ED* (a), (d), middle *ED* (b), (e) and high *ED* (c), (f) rods. (d)–(f) Enlarged images of the duplex region.

Table 1 *ED*, W_γ, $V_{\gamma\mathrm{dp}}$, V_{Ldp} and $V_{\alpha_2\mathrm{dp}}$ of low, middle and high *ED* rods with standard deviation of each value.

	ED (J/mm^3)	W_γ (µm)	$V_{\gamma\mathrm{dp}}$ (%)	V_{Ldp} (%)	$V_{\alpha_2\mathrm{dp}}$ (%)
Low ED	13	62(±10)	23(±10)	76(±10)	1(±0.2)
Middle ED	20	28(±4)	14(±3)	84(±3)	2(±0.2)
High ED	31	20(±5)	6(±2)	92(±2)	2(±0.3)

total width of the duplex region and γ band is approximately 90 µm for all rods, which is consistent with the layer thickness during the fabrications. On the other hand, Table 1 reveals the differences among the rods by comparing the morphology of the microstructure in each region. The width of the γ band (W_γ) decreases with increasing *ED*. W_γ of the low *ED* rod is approximately 62 µm, whereas those of the medium and high *ED* rods are approximately 28 µm and 20 µm, respectively (Table 1). Moreover, an interesting trend is observed for the volume fraction of equiaxed γ grains ($V_{\gamma\mathrm{dp}}$) and α_2/γ lamellar grains (V_{Ldp}) in the duplex region. As summarized in Table 1, $V_{\gamma\mathrm{dp}}$ decreases from approximately 23% (low *ED* rod) to 6% (high *ED* rod) and V_{Ldp} increases from approximately 76% (low *ED* rod) to 92% (high *ED* rod) with increasing *ED*. It is also noted that the volume fraction of fine granular α_2 phase ($V_{\alpha_2\mathrm{dp}}$) is approximately 1–2% in all rods. These results indicate that the morphology of the unique layered microstructure depends strongly on *ED*, especially increasing *ED* decreases the volume fraction of the γ phase in the microstructure.

To understand influence of *ED* on the variation of morphology of the layered microstructure, it is important to focus on the microstructural evolution during the EB-PBF process. Previous studies have demonstrated that the layered microstructure is formed via the following process (Fig. 3(a)).[37,43)]

STEP 1. A temperature distribution is generated at the vicinity of the melt pool during the electron beam scanning. The temperature distribution results in formation of a gradient microstructure near top surface of the rod. The type of the microstructure at each area depends on the temperature at the area.[43)]

STEP 2. 90 µm of new powder layer is raked.

STEP 3. A new gradient microstructure is formed near new top surface of the rod owing to the thermal effect from the melt pool as the new powder is melted. Then, the gradient microstructure formed in STEP 1 is partly replaced by the new gradient microstructure. However, the duplex and near γ structures remain at the area with a thickness of 90 µm corresponding to the layer thickness, where the thermal effect from melt pool does not reach.

STEP 4. Thereafter, the powder raking (STEP 2) and melting (STEP 3) steps are repeated, resulting in formation of the layered microstructure in which the duplex region and the γ band appear alternately.

In other words, the gradient microstructure caused by the thermal effect from the melt pool is a crucial factor leading to the formation of the layered microstructure. In the case of laser beam powder bed fusion (LB-PBF), the area exposed to the thermal effect from the melt pool is narrower than that of EB-PBF. Therefore, it is difficult to obtain 4822 alloys with the layered microstructure.[46)] The morphologies of the gradient microstructure such as width of each structure and volume fraction of each phase depend significantly on the temperature distribution around the melt pool. The temperature distribution shifts toward higher temperatures with increasing *ED*, resulting in broadening of the lamellar and duplex structures and narrowing of the near γ structure (Fig. 3(b)). An increase in *ED* also causes a decrease and an increase in the volume fraction of the equiaxed γ and the α_2/γ lamellar grains in the duplex structure, respectively. It is supposed that these morphological changes in the gradient microstructure formed near top surface of the rod during the process are responsible for the difference in microstructure between high *ED* and low *ED* rods.

3.2 Relationship between microstructure and tensile properties

It was found that the morphology of the unique layered microstructure observed in 4822 alloy rods prepared by EB-PBF depends strongly on *ED*. The differences in microstructural morphology are closely related to the mechanical properties of the rods. Figure 4 shows σ_y and *EL* of low, middle and high *ED* rods deformed at room temperature. σ_y increases from approximately 510 MPa (low *ED* rod) to 620 MPa (high *ED* rod) and *EL* decreases from approximately 1% (low *ED* rod) to 0.4% (high *ED* rod) with increasing *ED*. The strength-ductility balance of the rods fabricated by EB-PBF is better than that of HIP treated cast alloys (σ_y: approximately 380–500 MPa, *EL*: approximately 0.5%).[47)] Furthermore, it should be mentioned, low and high *ED* rods exhibit particularly high ductility and high strength, respectively, compared with the conventional alloys. It should be noted that the tensile properties were uniform from the bottom to the top of rods since no height dependence was observed in the microstructure of each rod.

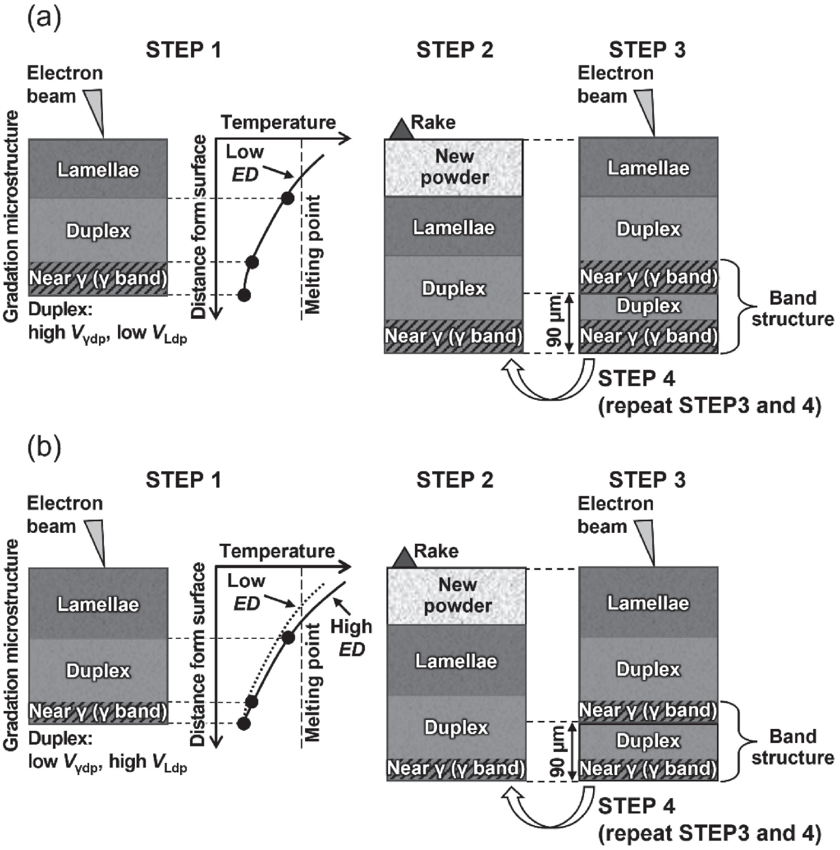

Fig. 3 Illustrations showing evolution of unique layered microstructure of the 4822 alloy rods fabricated at low (a) and high (b) *ED* conditions.

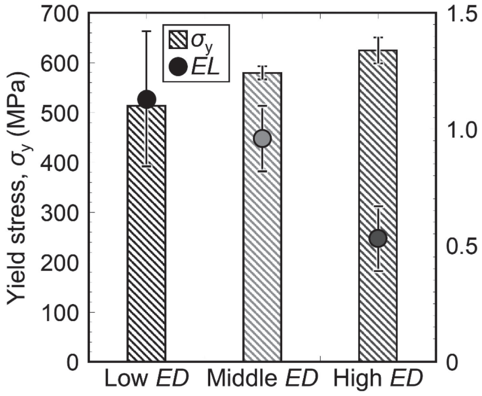

Fig. 4 σ_y and *EL* of low, middle and high *ED* rods deformed at room temperature.

The relationship between the microstructure and mechanical properties was investigated to understand the difference in the tensile properties of each rod. The nanoindentation hardness of the duplex region in each sample is shown in Fig. 5(a) along with that of the respective γ band. Regardless of the process conditions, the hardness of the γ band is approximately 3.5 GPa for all samples, whereas the duplex region harden from approximately 4 GPa (low *ED* rod) to 5 GPa (high *ED* rod) with increasing *ED*. This result suggests that the γ band is always softer than the duplex region. Therefore, the γ band is primarily responsible for elongation of the rods. This is consistent with the fact that a uniform fine near γ structure contributes to an excellent ductility of the 4822 alloys fabricated by LB-PBF.[46] The hardening of the duplex region with increasing *ED* is due to a decrease in the deformable equiaxed γ grains and an increase in the hard α_2/γ lamellar grains in the duplex region (Fig. 5(b)). This hardening of the duplex region should be involved in improvement of the strength of the alloys. Therefore, it is supposed that the strength of the alloys with the layered microstructure is affected by W_γ and V_{Ldp}, while the ductility depends on W_γ and $V_{\gamma dp}$. Figure 6 shows relationships between tensile properties of the rods and the morphology of the microstructure. The decrease in W_γ and the increase in V_{Ldp} are important for the strengthening of the alloys. In contrast, both W_γ and $V_{\gamma dp}$ should be increased for achieving high ductility alloys.

4. Conclusions

The influence of input energy density on the morphology of the layered microstructure of 4822 alloys fabricated by EB-PBF was investigated. In addition, relationships between the microstructure and mechanical properties of the rods were discussed focusing on the hardness and volume fraction of each constituent structure. The following conclusions were drawn from the present study:

(1) The γ band becomes narrower with increasing *ED*. In the duplex region, the volume fractions of the equiaxed γ and α_2/γ lamellar grains decrease and increase with increasing *ED*, respectively. This is because the

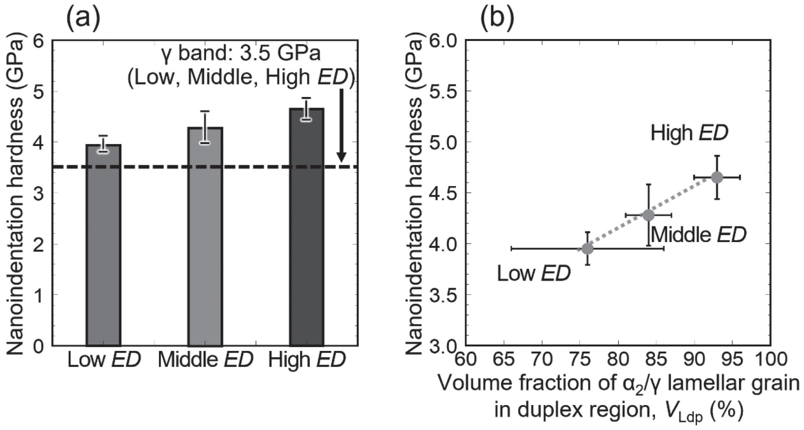

Fig. 5 Nanoindentation hardness of the duplex region of low, middle and high *ED* rods (a) and valuation in nanoindentation hardness of the duplex region as a function of V_{Ldp} (b).

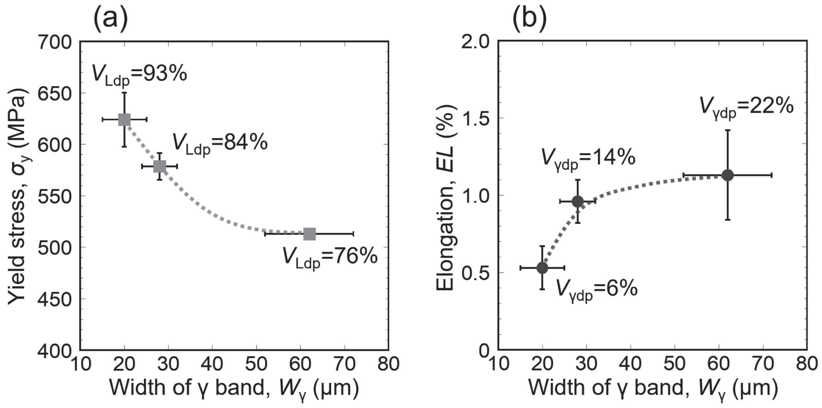

Fig. 6 Relationships between σ_{y} and W_{γ}, V_{Ldp} (a) and between EL and W_{γ}, $V_{\gamma\mathrm{dp}}$ (b) for the 4822 alloy rods with unique layered microstructure.

temperature distribution around the melt pool shifts toward higher temperatures with increasing *ED*.

(2) The mechanical properties of the 4822 alloys with the layered microstructure can be controlled by varying *ED*. Low and high *ED* conditions result in high ductility and high strength, respectively.

(3) A narrow γ band and an increase in the volume fraction of the α_2/γ lamellar grains in the duplex region are effective in increasing the alloy strength. On the other hand, increases in the width of the γ band and volume fraction of the γ grains in the duplex region contribute to an increase in the alloy ductility.

(4) It is expected that TiAl alloy parts with excellent mechanical properties can be realized by optimizing the process conditions with regard to *ED* on the basis of relationships between "*ED* and microstructure" and "microstructure and mechanical properties" revealed in this study.

Acknowledgments

This study was supported by the Council for Science, Technology and Innovation (CSTI), Cross-ministerial Strategic Innovation Promotion Program (SIP) from the Japan Science and Technology Agency (JST), Japan. This work was also partly supported by JSPS KAKENHI Grant Number JP21H05196, the Light Metal research Foundation, the Light Metal Educational Foundation and Frontier Research Grants, the Japan Institute of Metals and Materials.

REFERENCES

1) W.E. Frazier: J. Mater. Eng. Perform. **23** (2014) 1917–1928.
2) J.J. Lewandowski and M. Seifi: Annu. Rev. Mater. Sci. **46** (2016) 151–186.
3) T. Nakano, T. Ishimoto, R. Ozasa and A. Matsugaki: J. Therm. Spray Technol. **58** (2021) 121–128 (in Japanese).
4) L. Nickels: Met. Powder Rep. **70** (2015) 300–303.
5) T. Nakano: J. JILM **67** (2017) 470–480 (in Japanese).
6) W.S.W. Harun, M.S.I.N. Kamariah, N. Muhamad, S.A.C. Ghani, F. Ahmad and Z. Mohamed: Powder Technol. **327** (2018) 128–151.
7) B. Dutta and F.H. (Sam)Froes: Met. Powder Rep. **72** (2017) 96–106.
8) N. Ikeo, H. Fukuda, A. Matsugaki, T. Inoue, A. Serizawa, T. Matsuzaka, T. Ishimoto, R. Ozasa, O. Gokcekaya and T. Nakano: Crystals **11** (2021) 959.
9) K. Yamanaka, A. Kuroda, M. Ito, M. Mori, H. Bian, T. Shobu, S. Sato and A. Chiba: Addit. Manuf. **37** (2021) 101678.
10) E. Chauvet, P. Kontis, E.A. Jägle, B. Gault, D. Raabe, C. Tassin, J.-J. Blandin, R. Dendievel, B. Vayre, S. Abed and G. Martin: Acta Mater. **142** (2018) 82–94.
11) S.H. Sun, Y. Koizumi, T. Saito, K. Yamanaka, Y.-P. Li, Y. Cui and A. Chiba: Addit. Manuf. **23** (2018) 457–470.
12) I.-T. Ho, T.-H. Hsu, Y.-J. Chang, C.-W. Li, K.-C. Chang, S. Tin, K.

Kakehi and A.-C. Yeh: Addit. Manuf. **35** (2020) 101328.
13) I. Tolosa, F. Garciandía, F. Zubiri, F. Zapirain and A. Esnaola: Int. J. Adv. Manuf. Technol. **51** (2010) 639–647.
14) M.S.F. de Lima and S. Sankaré: Mater. Des. **55** (2014) 526–532.
15) L.E. Murr, S.M. Gaytan, A. Ceylan, E. Martinez, J.L. Martinez, D.H. Hernandez, B.I. Machado, D.A. Ramirez, F. Medina, S. Collins and R.B. Wicker: Acta Mater. **58** (2010) 1887–1894.
16) M. Seifi, A.A. Salem, D.P. Satko, Ulf. Ackelid, S.L. Semiatin and J.J. Lewandowski: J. Alloy. Compd. **729** (2017) 1118–1135.
17) K. Inoue and K. Kakehi: J. JILM **71** (2021) 214–216 (in Japanese).
18) M. Todai, T. Nagase, T. Hori, A. Matsugaki, A. Sekita and T. Nakano: Scr. Mater. **129** (2017) 65–68.
19) T. Kurzynowski, K. Gruber, W. Stopyra, B. Kuźnicka and E. Chlebus: Mater. Sci. Eng. A **718** (2018) 64–73.
20) S.-H. Sun, T. Ishimoto, K. Hagihara, Y. Tsutsumi, T. Hanawa and T. Nakano: Scr. Mater. **159** (2019) 89–93.
21) T. Hori, T. Nagase, M. Todai, A. Matsugaki and T. Nakano: Scr. Mater. **172** (2019) 83–87.
22) O. Gokcekaya, N. Hayashi, T. Ishimoto, K. Ueda, T. Narushima and T. Nakano: Addit. Manuf. **36** (2020) 101624.
23) A.D. Kudzal, B.A. McWilliams, J. Taggart-Scarff and M. Knezevic: Mater. Sci. Eng. A **770** (2020) 138512.
24) K. Hagihara, T. Ishimoto, M. Suzuki, R. Ozasa, A. Matsugaki, P. Wang and T. Nakano: Scr. Mater. **203** (2021) 114111.
25) Y. Iijima, T. Nagase, A. Matsugaki, P. Wang, K. Ameyama and T. Nakano: Mater. Des. **202** (2021) 109548.
26) T. Ishimoto, R. Ozasa, K. Nakano, M. Weinmann, C. Schnitter, M. Steele, A. Matsugaki, T. Nagase, T. Matsuzaka, M. Todai, H.S. Kim and T. Nakano: Scr. Mater. **194** (2021) 113658.
27) T. Todo, T. Ishimoto, O. Gokcekaya, J. Oh and T. Nakano: Scr. Mater. **206** (2022) 114252.
28) T. Ishimoto, K. Hagihara, K. Hisamoto, S.-H. Sun and T. Nakano: Scr. Mater. **132** (2017) 34–38.
29) C.A. Biffi, J. Fiocchi, E. Ferrario, A. Fornaci, M. Riccio, M. Romeo and A. Tuissi: J. Adv. Manuf. Technol. **107** (2020) 4913–4924.
30) T. Ishimoto, K. Hagihara, K. Hisamoto and T. Nakano: Addit. Manuf. **43** (2021) 102004.
31) A. Takase, T. Ishimoto, R. Suganuma and T. Nakano: Scr. Mater. **201** (2021) 113953.
32) S.-H. Sun, K. Hagihara, T. Ishimoto, R. Suganum, Y.-F. Xue and T. Nakano: Addit. Manuf. **47** (2021) 102329.
33) A. Takase, T. Ishimoto, R. Suganuma and T. Nakano: Addit. Manuf. **47** (2021) 102257.
34) S.-H. Sun, K. Hagihara and T. Nakano: Mater. Des. **140** (2018) 307–316.
35) Y.S. Lee, M.M. Kirka, J. Ferguson and V.C. Paquit: Addit. Manuf. **32** (2020) 101031.
36) O. Gokcekaya, T. Ishimoto, S. Hibino, J. Yasutomi, T. Narushima and T. Nakano: Acta Mater. **212** (2021) 116876.
37) M. Todai, T. Nakano, T. Liu, H.Y. Yasuda, K. Hagihara, K. Cho, M. Ueda and M. Takeyama: Addit. Manuf. **13** (2017) 61–70.
38) K. Cho, R. Kobayashi, J.Y. Oh, H.Y. Yasuda, M. Todai, T. Nakano, A. Ikeda, M. Ueda and M. Takeyama: Intermetallics **95** (2018) 1–10.
39) K. Cho, R. Kobayashi, T. Fukuoka, J.Y. Oh, H.Y. Yasuda, M. Todai, T. Nakano, A. Ikeda, M. Ueda and M. Takeyama: Sci. Forum **941** (2018) 1597–1602.
40) M. Sakata, J.Y. Oh, K. Cho, H.Y. Yasuda, M. Todai, T. Nakano, A. Ikeda, M. Ueda and M. Takeyama: Mater. Sci. Forum **941** (2018) 1366–1371.
41) K. Cho, H. Kawabata, T. Hayashi, H.Y. Yasuda, H. Nakashima, M. Takeyama and T. Nakano: Addit. Manuf. **46** (2021) 102091.
42) K. Cho, H. Odo, K. Okamoto, H.Y. Yasuda, H. Nakashima, M. Takeyama and T. Nakano: Crystals **11** (2021) 809.
43) H.Y. Yasuda, K. Cho, M. Todai, M. Ueda, D. Kondo, S. Morokoshi, A. Ikeda, M. Takeyama and T. Nakano: J. Smart Process. **8** (2019) 78–83 (in Japanese).
44) P. Karimi, E. Sadeghi, J. Ålgårdh and J. Andersson: Mater. Charact. **148** (2019) 88–99.
45) Y. Zhao, K. Aoyagi, K. Yamanaka and A. Chiba: Addit. Manuf. **36** (2020) 101559.
46) K. Mizuta, Y. Hijikata, T. Fujii, K. Gokan and K. Kakehi: Scr. Mater. **203** (2021) 114107.
47) J. Han, J. Dong, S. Zhang, C. Zhang, S. Xiao and Y. Chen: Mater. Sci. Eng. A **715** (2018) 41–48.